Supporting information

Direct synthesis of methyl acetate and acetic acid from syngas over tandem catalysts composed of a Cu-based catalyst and a Cu-exchanged mordenite zeolite

Katsuya Shimura*, Isao Nakamura, Tadahiro Fujitani

Research Institute for Chemical Process Technology, National Institute of Advanced Industrial Science and Technology (AIST), 1-1-1 Higashi, Tsukuba, Ibaraki 305-8565, Japan

***Corresponding author**

Katsuya Shimura. E-mail: katsuya-shimura@aist.go.jp, Tel.: +8180-2339-4470

S1. Additional experimental details

S1.1. Catalyst characterization

Nitrogen adsorption–desorption: Measurements were made at −196 °C using a BELSORP MAX II (MicrotracBEL Corp.). Prior to measurement, 0.05 g of catalyst powder was degassed under vacuum at 350 °C for 4 h. Specific surface area was calculated via the Brunauer–Emmett–Teller (BET) method. Total pore volume was calculated from the amount of nitrogen gas adsorbed at a relative pressure of 0.99. Micropore volume and external specific surface area of the zeolite catalysts were calculated using the *t*-plot method. The pore size distribution was determined from the desorption branches of the N_2 isotherms using the Barrett–Joyner–Halenda (BJH) method.

X-ray diffraction (XRD): Cu-based catalysts were analyzed using a D8 ADVANCE diffractometer (Bruker AXS), and zeolites were analyzed using a D8 DISCOVER diffractometer (Bruker AXS), both using Cu Kα radiation (40 kV, 40 mA), 2θ = 10–70°, step 0.02°.

Metal content: The amounts of ion-exchanged metal on the zeolites were measured by ICP-AES (ICPE-9800; Shimadzu) after dissolving the sample in hydrofluoric acid at room temperature.

Field-emission scanning electron microscopy (FE-SEM): Images were recorded using a S-4800 microscope (Hitachi) at an accelerating voltage of 15 kV.

N_2O chemisorption: Cu dispersion was determined via N_2O pulse measurement using a BELCAT II auto-chemisorption instrument equipped with a thermal conductive detector (MicrotracBEL Corp.). Catalysts (0.01 g) were reduced at 350 °C for 1 h in a flow of H_2 (10%)/Ar (30 mL min^{-1}) and then held at 350 °C for 0.5 h in a flow of He (30 mL min^{-1}) to desorb the residual chemisorbed H_2. After cooling to 50 °C in flowing He, N_2O (10%)/He was pulsed over the catalyst until no N_2O adsorption was detected. Cu dispersion was calculated assuming 1:2 stoichiometry for adsorbed N_2O to surface Cu atoms.

UV-vis spectroscopy: Diffuse reflectance UV-vis spectra in the spectral range of 190–900 nm were recorded on a V-750 spectrometer (JASCO Corp.) equipped with an integrating sphere. $BaSO_4$ was used as a reference sample to measure the baseline spectrum.

NH_3 temperature-programed desorption (NH_3-TPD): NH_3-TPD was performed using a BELCAT II auto-chemisorption system. Catalysts (0.10 g) were mounted into a quartz cell and heated in flowing He (30 mL min^{-1}) at 500 °C for 1 h prior to analysis. The adsorption of NH_3 was performed at 100 °C for 0.5 h in flowing NH_3 (5%)/He (30 mL min^{-1}). Then, the catalyst was treated with He (30 mL min^{-1}) at 100 °C for 1 h to remove the physisorbed NH_3, and TPD was performed by heating the catalyst to 800 °C at a rate of 10 °C min^{-1} in flowing He (30 mL min^{-1}). Peak deconvolution was performed using Gaussian functions within the ChemMaster II analysis software (version 1.0.1; MicrotracBEL Corp.). BASs amounts were calculated from the area of the desorption peak centered at 550 °C.[1]

H_2 temperature-programmed reduction (H_2-TPR): H_2-TPR was performed using a BELCAT II auto-chemisorption system. Catalysts (0.10 g) were loaded into a quartz cell, and the temperature was increased to

800 °C (heating rate, 10 °C min^{-1}) under H_2 (10%)/Ar flow (30 mL min^{-1}). A downstream trap containing molecular sieve 5A was used to remove water formed during the analysis. The degree of Cu reduction was calculated from the amount of H_2 consumed.

Fourier transformed infrared (FT-IR) spectroscopy: O–H stretching of Cu-MOR catalysts was measured on a FT/IR-4700 spectrometer (JASCO Corp.) equipped with a TGS detector in transmission mode. The catalyst powders were pressed into self-supporting wafers (diameter 1 cm, weight 10 mg), placed into a sample holder, and loaded into an infrared cell with CaF_2 windows. After evacuation under a vacuum at 450 °C for 1 h, the sample was cooled to 200 °C, and the spectrum was recorded in the range of 4000–1200 cm^{-1} (256 scans, resolution 4 cm^{-1}). The background was recorded using KBr.

In situ diffuse reflectance infrared Fourier transform spectroscopy (DRIFTS): CO adsorption on Cu-MOR catalysts was recorded with a FT/IR-6600 spectrometer (JASCO Corp.) equipped with a diffuse reflectance attachment and a MCT detector. Samples were placed in an infrared cell equipped with ZnSe windows. Prior to measurement, the sample was reduced at 350 °C for 1 h in a flow of H_2 (33%)/N_2 (60 mL min^{-1}) and then held at 350 °C for 0.5 h in a flow of N_2 (40 mL min^{-1}) to desorb residual chemisorbed H_2. After the reduced catalyst was cooled to 100 °C in a flow of N_2, a background spectrum was recorded. Then, CO (10%)/He (10 mL min^{-1}) was fed to the cell for 10 min. After adsorption of CO, the cell was purged with N_2 for 10 min to remove gaseous CO and then the IR spectra were recorded (128 scans, 4 cm^{-1} resolution).

CO temperature-programmed desorption (CO-TPD): CO-TPD was performed with a BELCAT II auto-chemisorption instrument equipped with a mass spectrometer. Catalysts (0.10 g) were placed into quartz cells and reduced in flowing H_2 (10%)/Ar (30 mL min^{-1}) at 350 °C for 1 h and then held at 350 °C for 0.5 h in a flow of He (30 mL min^{-1}) to desorb residual chemisorbed H_2. The adsorption of CO was performed at 100 °C for 0.5 h in flowing CO (10%)/He (30 mL min^{-1}). Then, the catalyst was treated with He (30 mL min^{-1}) at 100 °C for 1 h to remove physisorbed CO, and TPD was performed by heating the catalyst to 800 °C at a rate of 10 °C min^{-1} in flowing He (30 mL min^{-1}).

Thermogravimetric analysis (TGA) was performed on a TG 209 F1 Libra® instrument (NETZSCH) at a heating rate of 10 °C min^{-1} in flowing O_2(21.4%)/He (50 mL min^{-1}). The products released from coke were detected by a combination of thermogravimetric analysis and mass spectrometry.

S2. Supplementary Results

Table S1 Previously reported tandem catalysts for the conversion of syngas to MA and AA

Entry	Catalyst	Reaction conditions				CO conv. (%)	Selectivity (%)		Ref.
		Temperature (°C)	Pressure (MPa)	H_2/CO ratio	GHSV (mL g^{-1} h^{-1})		CO_2	MA+AA	
1	Cu-Zn-Al/H-ZSM-5 | H-MOR	220	3.0	1	1500	10	21	77	2
2	$ZnAl_2O_4$ | H-MOR	370	3.0	2	1500	11	20	70	2
3	CuZnAl-HZSM-5 | Zn-HMOR	220	2.0	2	2000	6.8	–[a]	94.4[b]	3
4	$CuZnO_x$ | Cu-MOR | $CuZnO_x$	200	4.6	1	1081	8.1	8.3	0.3 (EtOH 20.2%)	4
5	K^+-ZnO-ZrO_2 | H-MOR-DA-12MR	310	5.0	1	1136	5.6	12	76	5
6	Cu/ZnAlMgO | H-MOR	210	2.5	4	3333	–[a]	–[a]	87[b]	6
7	Cu-ZnO-Al_2O_3 | H-FER	275	5.0	3.1	12500	41.7	–[a]	12.8[b]	7
8	$CuZnAlO_x$/γ-Al_2O_3 | Py-HMOR	270	2.0	2	7000	50	22	75	8
9	$CuZnAlO_x$/H-ZSM-5 | Py-MOR	280	4.0	1	1091	65	21	70	9
10	$CuMgAlO_x$ | Cu-MOR	230	5.0	2	3429	2.8	4.4	93.7	This work

[a] Not reported. [b] Excluding CO_2.

Table S2 Physicochemical properties of the CMA and CMYA catalysts before H_2 reduction

Cu catalyst	BET specific surface area ($m^2\ g^{-1}$)	Pore volume ($cm^3\ g^{-1}$)	Average pore size (nm)
CMA	105	0.54	20.5
CMYA	201	0.88	17.4

Table S3 Degree of Cu reduction on CMA and CMYA catalysts

Cu catalyst	Degree of Cu reduction [a] (%)
CMA	87
CMYA	111

[a] Degree of Cu reduction was calculated from the amount of H_2 consumed at below 350 °C using H_2-TPR profiles, assuming that Cu was deposited as CuO

Table S4 Dispersion, surface area, and particle size of Cu metal particles, as measured by N_2O pulse measurement

Cu catalyst	Cu loading (wt%)	Dispersion (%)	Surface area ($m^2\ g_{cat.}^{-1}$)	Particle size (nm)
CMA	38.8	2.6	6.6	39.6
CMYA	30.5	10.6	20.8	9.9

Table S5 Physicochemical properties of the metal ion-exchanged MOR zeolites

Entry	Catalyst	BET SSA[a] ($m^2\ g^{-1}$)	External SSA[a] ($m^2\ g^{-1}$)	V_{total}[b] ($cm^3\ g^{-1}$)	V_{micro}[c] ($cm^3\ g^{-1}$)	Average pore size (nm)
1	MOR(18)	522	16	0.238	0.197	1.83
2	Mg(1.2)-MOR(18)	508	25	0.246	0.174	1.94
3	Mn(3.2)-MOR(18)	475	20	0.232	0.177	1.96
4	Fe(4.7)-MOR(18)	506	23	0.250	0.181	1.97
5	Co(3.0)-MOR(18)	502	16	0.261	0.194	2.08
6	Ni(2.0)-MOR(18)	522	23	0.253	0.185	1.94
7	Cu(3.1)-MOR(18)	494	14	0.239	0.187	1.93
8	Zn(3.6)-MOR(18)	464	19	0.228	0.174	1.97
9	Ag(4.9)-MOR(18)	502	24	0.243	0.174	1.94
10	Cu(3.4)-MOR(15)	535	4	0.220	0.208	1.64
11	Cu(2.4)-MOR(30)	547	11	0.273	0.227	2.00
12	Cu(1.2)-MOR(90)	543	34	0.367	0.244	2.71
13	Cu(0.4)-MOR(240)	546	17	0.305	0.242	2.23

[a] SSA: Specific surface area. [b] Total pore volume. [c] Micropore volume.

Table S6 Peak deconvolution of the NH_3-TPD profiles of Cu-MOR

Catalyst	NH_3 desorption ($mmol\ g^{-1}$)			
	α	β	γ	δ
Cu(3.4)-MOR(15)	0.91	0.59	1.54	0.30
Cu(3.1)-MOR(18)	0.62	0.47	1.19	0.11
Cu(2.4)-MOR(30)	0.39	0.38	0.58	0.60
Cu(1.2)-MOR(90)	0.14	0.15	0.51	0.21
Cu(0.4)-MOR(240)	0.04	0.06	0.30	0.41

Table S7 Degree of Cu reduction on Cu-MOR

Catalyst	Degree of Cu reduction [a] (%)	
	Reduction at 350 ℃	Reduction at 800 ℃
Cu(2.4)-MOR(18)	64	100
Cu(2.7)-MOR(18)	65	102
Cu(3.1)-MOR(18)	63	97
Cu(3.7)-MOR(18)	61	101

[a] Degree of Cu reduction was calculated from the amount of H_2 consumed at below 350 °C or 800 °C in the H_2-TPR profiles, assuming that Cu was deposited as CuO.

Table S8 Conversion of syngas to MA and AA over the combination of CMYA and Cu(3.1)-MOR(18) catalysts at 220–250 °C [a]

Temperature (°C)	CO conv. (%)	Selectivity [b] (%)									Yield of MA+AA (%)	STY [c] of MA+AA (mmol g^{-1} h^{-1})
		CO_2	CH_4	C_{2-4} HC	C_{5-6} HC	MeOH	EtOH	MA	AA	DME		
220	3.4	2.5	0.3	0.4	0.0	5.6	0.0	35.7	0.0	55.8	1.20	0.21
230	4.9	8.5	0.4	0.5	0.0	3.4	0.0	60.8	4.0	23.7	3.17	0.58
240	5.0	6.9	2.4	5.1	1.8	4.0	0.0	54.5	2.9	20.8	2.89	0.53
250	4.5	14.3	14.5	39.7	8.8	0.0	0.0	0.8	7.9	0.0	0.39	0.10

[a] CMYA 0.5 g, Cu(3.1)-MOR(18) 2.0 g, 220–250 °C, 5 MPa, 340 min, Syngas 150 mL min^{-1}, N_2 50 mL min^{-1}.

[b] C_{2-4} HC: hydrocarbons with a carbon number of 2–4, C_{5-6} HC: hydrocarbons with a carbon number of 5–6, MA: methyl acetate, AA: acetic acid.

[c] STY: space-time yield.

Table S9 Conversion of syngas to MA and AA using the combination of CMA and Cu(3.1)-MOR(18) catalysts [a]

Amount of Cu-MOR (g)	CO conv. (%)	Selectivity [b] (%)									Yield of MA+AA (%)	STY [c] of MA+AA (mmol g^{-1} h^{-1})
		CO_2	CH_4	C_{2-4} HC	C_{5-6} HC	MeOH	EtOH	MA	AA	DME		
0.0	3.1	1.0	0.5	0.0	0.0	97.1	0.5	0.0	0.0	0.2	0.00	0.00
0.5	2.7	6.4	0.5	0.6	0.0	3.8	0.0	47.6	0.0	40.0	1.27	0.57
1.5	3.1	9.0	0.4	0.9	0.0	0.7	0.0	65.4	20.1	2.0	2.69	0.67
2.5	3.2	1.9	0.6	0.8	0.0	1.3	0.0	72.4	17.0	5.9	2.86	0.47
3.0	2.8	4.4	0.3	0.8	0.0	0.0	0.0	53.6	40.1	0.5	2.59	0.40

[a] CMA 0.5 g, Cu(3.1)-MOR(18) 0.0–3.0 g, 230 °C, 5 MPa, 340 min, Syngas 150 mL min^{-1}, N_2 50 mL min^{-1}.

[b] C_{2-4} HC: hydrocarbons with a carbon number of 2–4, C_{5-6} HC: hydrocarbons with a carbon number of 5–6, MA: methyl acetate, AA: acetic acid.

[c] STY: space-time yield.

Table S10 Conversion of syngas to MA and AA using the combination of CMA and Cu(3.1)-MOR(18) catalysts with different weight ratios [a]

Amount of catalyst (g)		CO conv. (%)	Selectivity [b] (%)									Yield of MA + AA (%)	STY [c] of MA+AA (mmol g^{-1} h^{-1})
CMA	Cu-MOR		CO_2	CH_4	C_{2-4} HC	C_{5-6} HC	MeOH	EtOH	MA	AA	DME		
2.00	1.00	7.9	6.4	0.5	0.4	0.0	6.6	0.0	9.6	0.0	75.7	0.76	0.11
1.00	2.00	4.9	4.6	0.6	0.6	0.0	4.6	0.0	45.4	0.0	42.8	2.22	0.33
0.75	2.25	4.1	6.1	0.4	0.7	0.0	2.0	0.0	69.0	9.3	12.5	3.22	0.51
0.50	2.50	3.2	1.9	0.6	0.8	0.0	1.3	0.0	72.4	17.0	5.9	2.86	0.47

[a] CMA 2.0–0.5 g, Cu(3.1)-MOR(18) 1.0–2.5 g, 230 ℃, 5 MPa, 340 min, Syngas 150 mL min^{-1}, N_2 50 mL min^{-1}.

[b] C_{2-4} HC: hydrocarbons with a carbon number of 2–4, C_{5-6} HC: hydrocarbons with a carbon number of 5–6, MA: methyl acetate, AA: acetic acid.

[c] STY: space-time yield.

Table S11 Effect of GHSV on CO conversion and product selectivity over the combination of CMA and Cu(3.1)-MOR(18) catalysts

GHSV (mL g^{-1} h^{-1})	CO conv. (%)	Selectivity (%)									Yield of MA + AA (%)	STY [c] of MA+AA (mmol g^{-1} h^{-1})
		CO_2	CH_4	C_{2-4} HC	C_{5-6} HC	MeOH	EtOH	MA	AA	DME		
1000	3.9	15.0	0.9	7.5	0.0	0.8	0.0	66.4	8.0	1.7	2.88	0.15
2000	3.2	7.0	0.6	1.4	0.0	0.9	0.0	77.0	10.6	2.3	2.80	0.29
3000	3.1	4.1	0.4	0.7	0.0	1.7	0.0	79.1	6.6	7.2	2.65	0.41
4000	3.0	2.5	0.4	0.6	0.0	2.5	0.0	72.9	6.1	15.5	2.38	0.49

[a] CMA 0.5 g, Cu(3.1)-MOR(18) 2.5 g, 230 ℃, 5 MPa, 340 min, Syngas 50–200 mL min^{-1}.

[b] C_{2-4} HC: hydrocarbons with a carbon number of 2–4, C_{5-6} HC: hydrocarbons with a carbon number of 5–6, MA: methyl acetate, AA: acetic acid.

[c] STY: space-time yield.

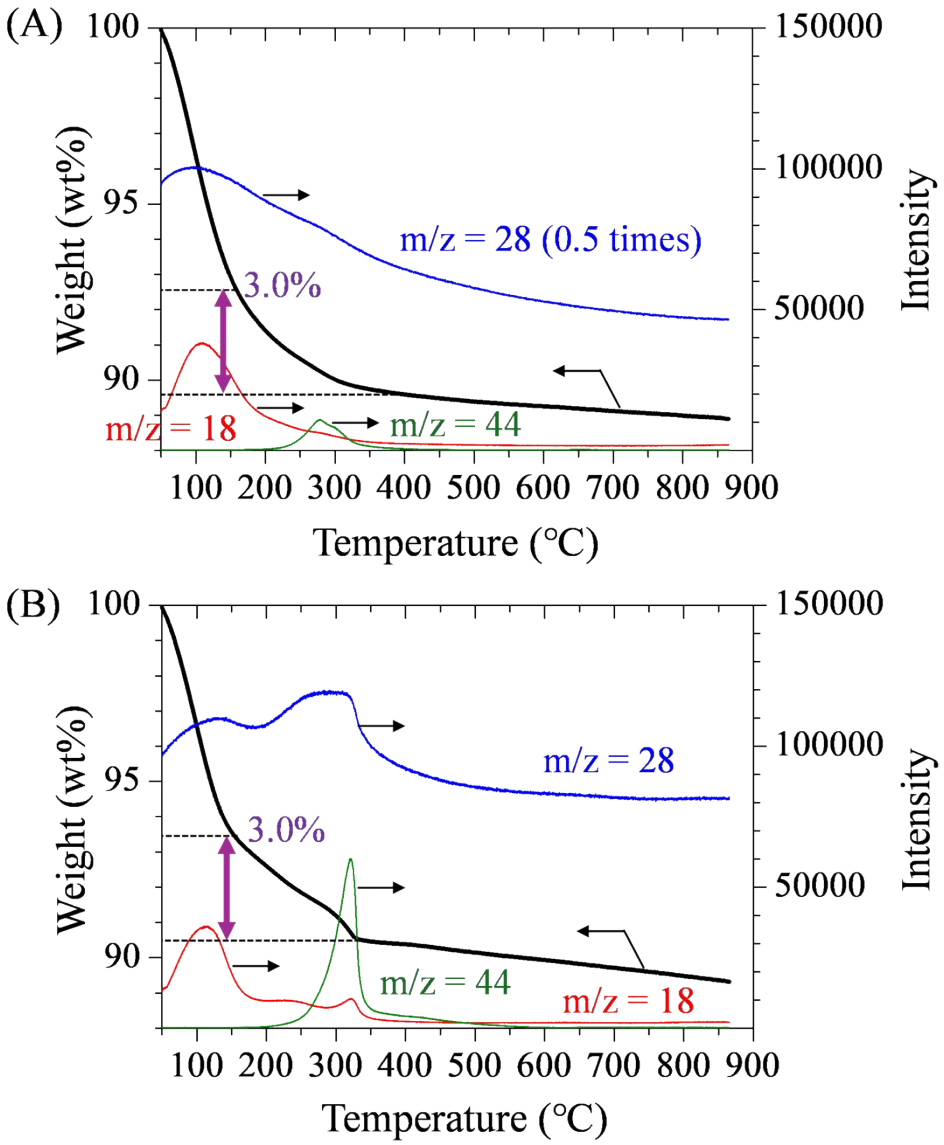

Fig. S1. TG-MS curves of the Cu(3.1)-MOR(18) catalyst after different time-on-stream: (A) 5 h and (B) 10 h.

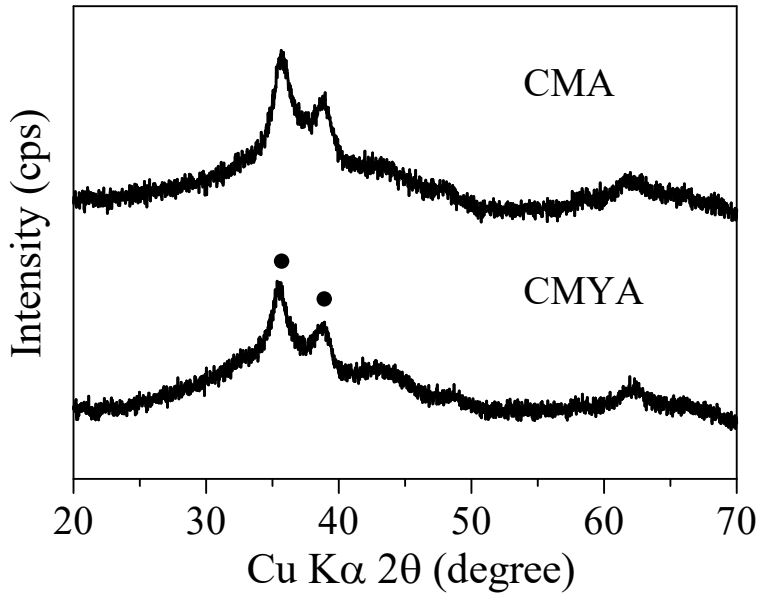

Fig. S2. XRD patterns of the CMA and CMYA catalysts before H_2 reduction. Black circles represent the diffraction lines of CuO.

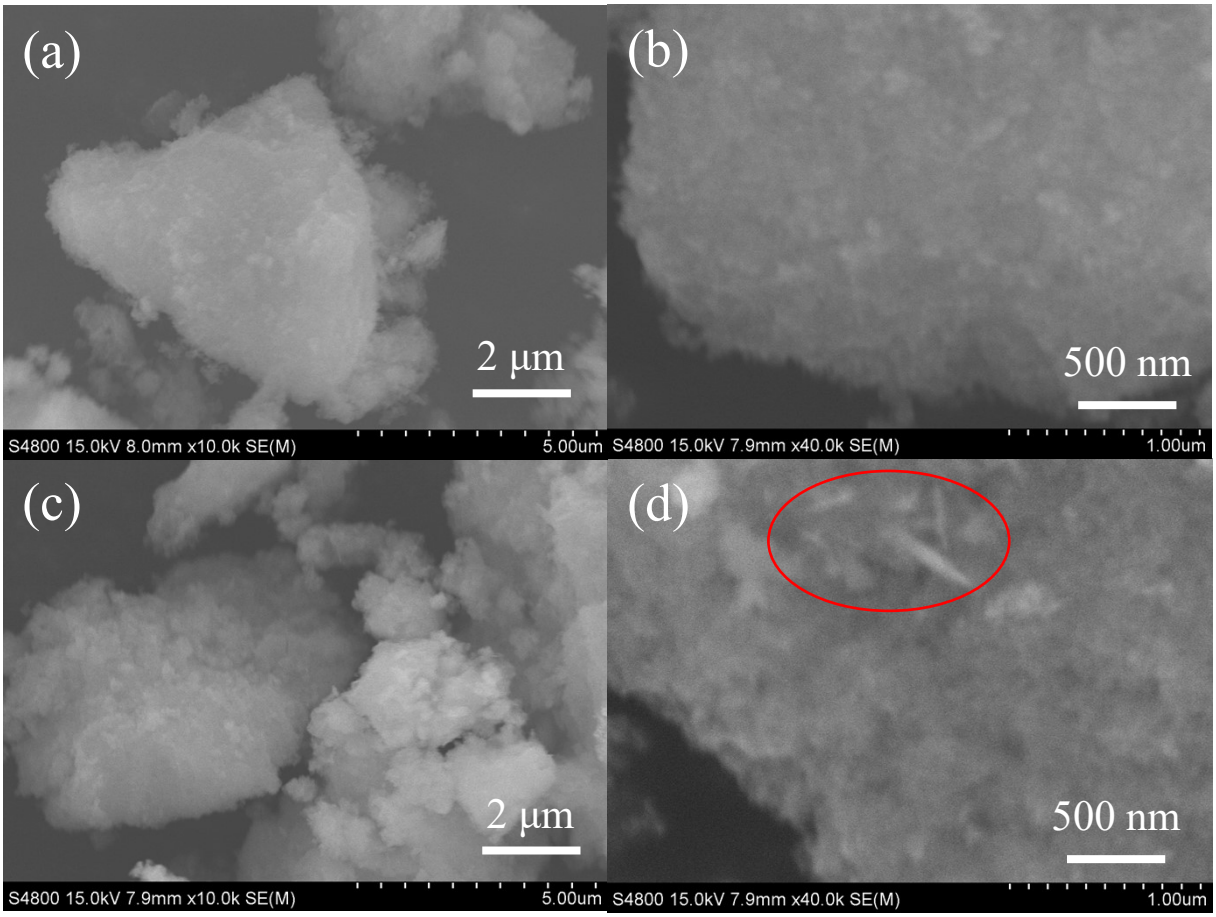

Fig. S3. FE-SEM images of the (a, b) CMA and (c, d) CMYA catalysts before H_2 reduction.

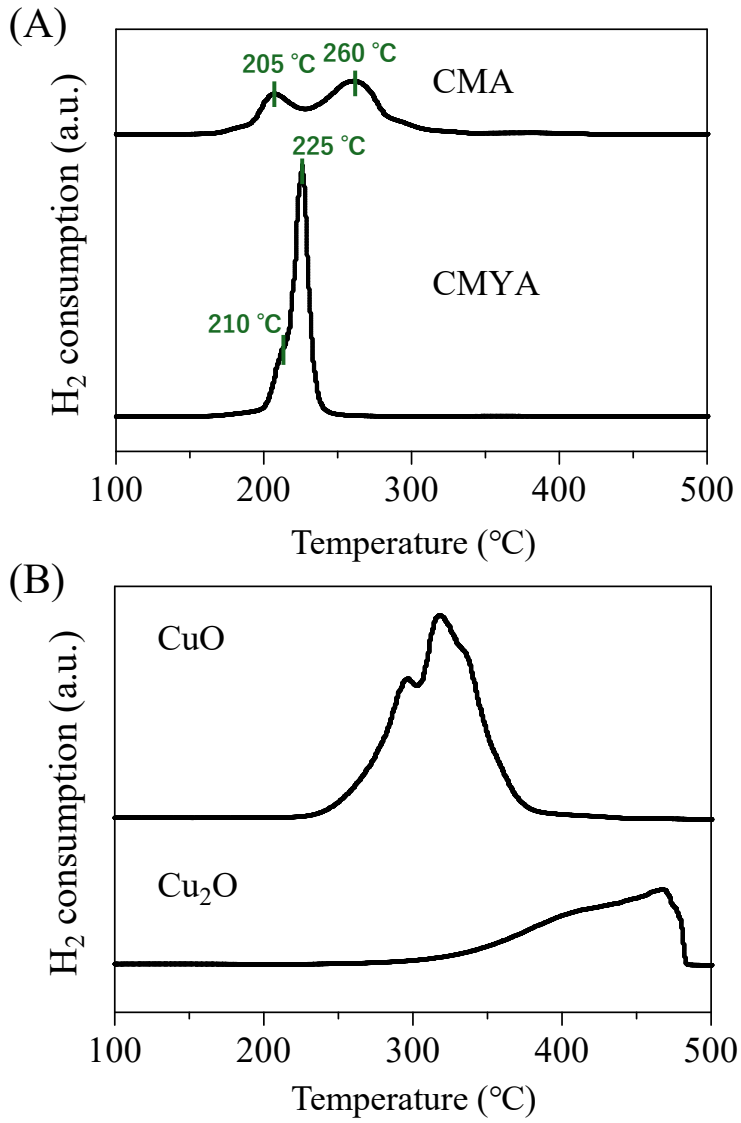

Fig. S4. H_2-TPR profiles of (A) the CMA and CMYA catalysts and (B) two references samples.

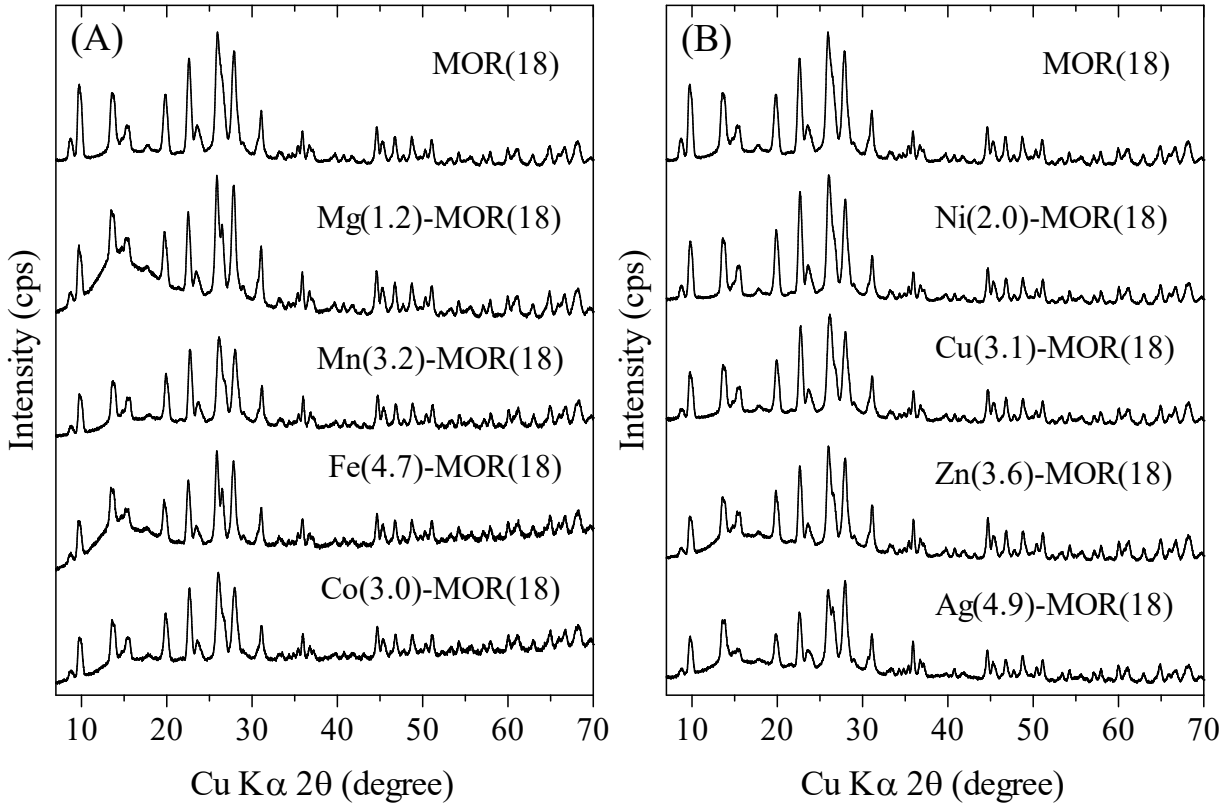

Fig. S5. XRD patterns of metal ion-exchanged MOR zeolites.

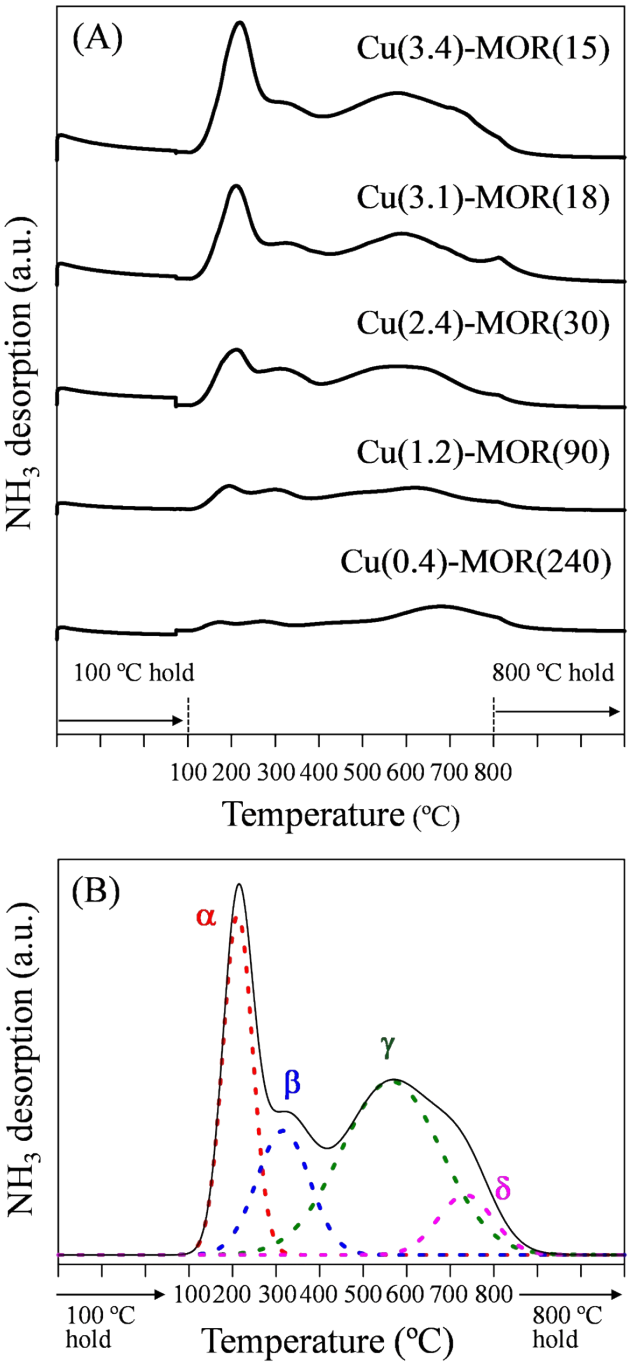

Fig. S6. (A) NH_3-TPD profiles of Cu-MOR catalysts and (B) curve fitting of the profile of the Cu(3.4)-MOR(15) catalyst.

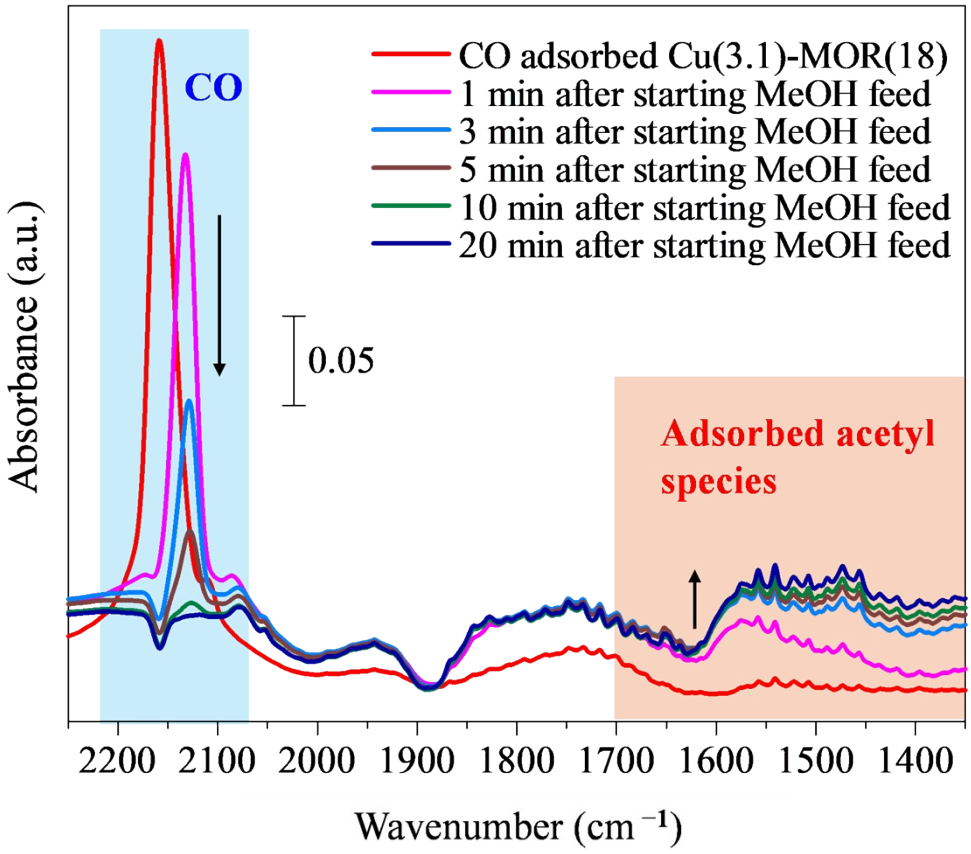

Fig. S7 In-situ DRIFT spectra of CO adsorbed on the Cu(3.1)-MOR(18) catalyst before and after MeOH feed. The spectra were recorded at 100 ℃ and 0.1 MPa. Methanol vapor was introduced into the cell by bubbling liquid methanol with N_2 gas (50 mL min^{-1}) at 20 ℃.

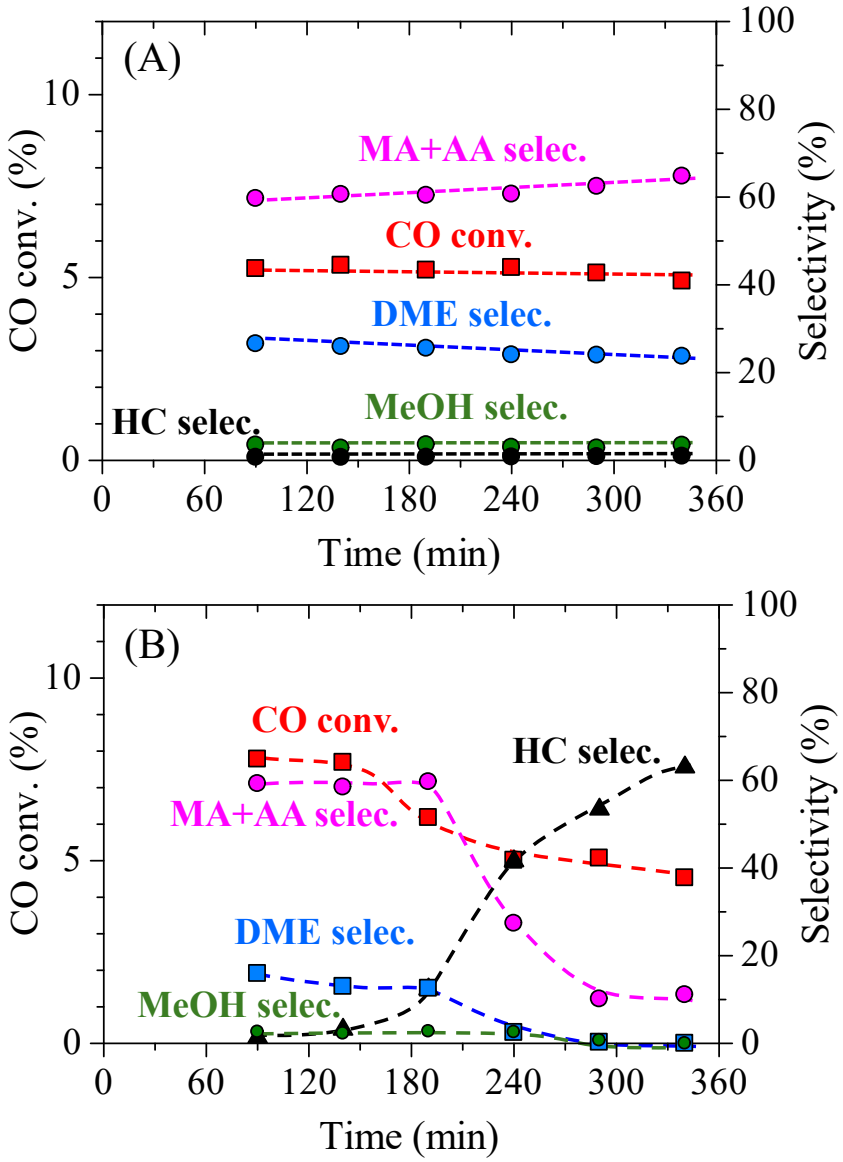

Fig. S8. Time course of CO conversion and product selectivity over the combination of CMYA and Cu(3.1)-MOR(18) catalysts at (A) 230 ℃ and (B) 250 ℃. Reaction conditions: CMYA 0.5 g, Cu-MOR(18) 2.0 g, 230 or 250 ℃, 5 MPa, Syngas 150 mL min^{-1}, N_2 50 mL min^{-1}.

S3. Supplementary References

1. Y. Liu, J. Qi, K. Zhu, H. Liu, X. Liu, M. Wang, M. Wang, J. Lv, S. Huang and X. Ma, *Catal. Sci. Technol.*, 2025, **15**, 2510–2518.
2. W. Zhou, J. Kang, K. Cheng, S. He, J. Shi, C. Zhou, Q. Zhang, J. Chen, L. Peng, M. Chen and Y. Wang, *Angew. Chem. Int. Ed.*, 2018, **57**, 12012–12016.
3. Z. Cao, T. Hu, J. Guo, J. Xie, N. Zhang, J. Zheng, L. Che and B.H. Chen, *Fuel*, 2019, **254**, 115542.
4. Y. Zhang, C. Ding, J. Wang, Y. Jia, Y. Xue, Z. Gao, B. Yu, B. Gao, K. Zhang and P. Liu, *Catal. Sci. Technol.*, 2019, **9**, 1581–1594.
5. J. Kang, S. He, W. Zhou, Z. Shen, Y. Li, M. Chen, Q. Zhang and Y. Wang, *Nature Commun.*, 2020, **11**, 827.
6. D.C. Upham, M. Orazov and T.F. Jaramillo, *J. Catal.*, 2021, **399**, 132–141.
7. W.C. Sung, H.S. Jung, J.W. Bae, J.Y. Kim and D.H. Lee, *J. CO_2 Util.*, 2023, **69**, 102411.
8. S. Han, D. Fan, N. Chen, W. Cui, L. He, P. Tian and Z. Liu, *ACS Catal.*, 2023, **13**, 10651−10660.
9. S. Liu, G. Wu, Y. Chen, Y. Han, M. Zhang, J. Kang, M. Tang, K.P. de Jong, Q. Zhang, Y. Wang and K. Cheng, *AIChE J.*, 2025, **71**, e18664.